

# All-dielectric Phase-gradient Metasurface Performing High-efficiency Anomalous Transmission in the Near-infrared Region

**Tiesheng Wu**

Key laboratory of optoelectronic device and systems if nubustry of education and guangdong province,shenzhen university

**Zhihui Liu** (✉ [zhihuil\\_guet@163.com](mailto:zhihuil_guet@163.com))

GUET: Guilin University of Electronic Technology <https://orcid.org/0000-0002-1814-5342>

**Yiping Wang**

Shenzhen University

**Huixian Zhang**

Guilin University of Electronic Technology

**Zuning Yang**

Guilin University of Electronic Technology

**Dan Yang**

Guilin University of Electronic Technology

---

**Nano Express**

**Keywords:** metasurface, phase gradient, anomalous transmission, all-dielectric

**Posted Date:** December 3rd, 2020

**DOI:** <https://doi.org/10.21203/rs.3.rs-117469/v1>

**License:** © ⓘ This work is licensed under a Creative Commons Attribution 4.0 International License.

[Read Full License](#)

---

## RESEARCH

# All-dielectric phase-gradient metasurface performing high-efficiency anomalous transmission in the near-infrared region

Tiesheng Wu<sup>1,2,3</sup>, Zhihui Liu<sup>2\*</sup>, Yiping Wang<sup>1,3\*</sup>, Huixian Zhang<sup>2</sup>, Zuning Yang<sup>2</sup> and Dan Yang<sup>2</sup>

## Abstract

We propose and numerically demonstrate a phase-gradient metasurface with high anomalous transmission efficiency and great anomalous refraction angle, which consists of discontinuous regular hexagonal nanorods supported by a quartz substrate. The metasurface achieves high anomalous transmission efficiency and full  $2\pi$  phase shift for the wavelength range of 1400-1600 nm. At the central wavelength around 1504 nm, the total transmission efficiency reaches 97.9%, and the desired anomalous transmission efficiency is up to 96.1% with an anomalous refraction angle as large as  $30.09^\circ$ . By adjusting the period and the number of nanorods in one unit cell, the anomalous refraction angle can reach  $68.03^\circ$ , and the anomalous transmission efficiency exceeds 60% within a bandwidth of 50 nm. The results are more excellent than those of most present phase-gradient metasurface structures. The superior performance of the proposed structure may pave the way for its application in wavefront control optical devices.

**Keywords:** metasurface; phase gradient; anomalous transmission; all-dielectric

## Introduction

In the past few years, because metasurface has the ability to modulate the characteristics of electromagnetic waves, such as polarization, phase, amplitude, and frequency through sub-wavelength microstructures. It has attracted a lot of attention in nanophotonics [1-7]. In 2005, Nicholas demonstrated a new class of metasurface optical devices based on the lo-

cal phase modulation effect of Surface Plasma (SP) [8]. Based on the characteristic of the SP propagation constant varies with the metal slot's width, flexible local phase regulation is realized, and the metasurface refraction law, also known as generalized refraction law, is established [9-12]. In 2011, Capasso's team built a new metasurface structure as a v-shaped antenna, this work further clarified the concept of the general law of refraction and resulted in an international research craze [13]. For example, converters [14-16], deflectors [9,17-20], directional surface wave couplers [21-23], holographic devices [24-26], vortex beam generators [27-29], and planar virtual excipient device [30], etc. According to the materials used in metasurfaces, we can divide optical metasurfaces into plasmonic metasurfaces and dielectric metasurfaces. Although the applica-

\*Correspondence: zhihuil.guet@163.com; ypwang@szu.edu.cn

<sup>2</sup>Guangxi Key Laboratory of Wireless Broadband Communication and Signal Processing, School of Information and Communication, Guilin University of Electronic Technology, Guilin 541004, China

<sup>1</sup>Key Laboratory of Optoelectronic Devices and Systems of Ministry of Education and Guangdong Province, Shenzhen University, Shenzhen 518060, China

<sup>3</sup>Key Laboratory of Optoelectronic Devices and Systems of Ministry of Education and Guangdong Province, College of Optoelectronic Engineering, Shenzhen University, Shenzhen 518060, China  
Full list of author information is available at the end of the article

tion prospect of plasmonic metasurfaces has been verified in many fields, the performance of this type of device is usually limited by the huge intrinsic ohmic loss of metal material [31,32]. Because of dielectric materials have very low inherent loss, people tried to replace metal materials with dielectric materials for designing all-dielectric metasurface [33, 34].

More recently, the common defect of the all-dielectric phase-gradient metasurface is that it is difficult to obtain high anomalous transmission efficiency with a large anomalous refraction angle. To solve this problem, Yang *et al.* designed an all-dielectric metasurface based on silicon nanoantennas for high-efficiency anomalous transmission, its anomalous transmission efficiency can reach 80.5% with an anomalous refraction angle of  $29.62^\circ$  [35]. In 2019, by using of cross-shaped structure, the anomalous transmission efficiency of the all-dielectric metasurface is up to 83.5% with an anomalous refraction angle of  $30^\circ$  [36]. As far as we know, it is the best result reported in the literature.

In this work, we demonstrate a novel all-dielectric phase-gradient metasurface, which consists of discontinuous regular hexagonal silicon nanorods supported by a quartz substrate. We systematically analyze the anomalous transmission efficiency and the anomalous refraction angle of the proposed structure by using the finite-difference time-domain (FDTD) method. The simulation results show that at the central wavelength of 1504 nm, the total transmission efficiency of the dielectric metasurface can reach 97.9%, and the section of the desired anomalous transmission efficiency is up to 96.1% with an anomalous refraction angle of  $30.09^\circ$ . The anomalous refraction angle can be enlarged by changing the number of elements in one unit cell and the period. We demonstrate an anomalous refraction angle reaches  $68.03^\circ$  with an anomalous transmission efficiency as high as 67.9% for the central wavelength of 1530 nm. The performance of the proposed structure is better than that of the previously reported phase-gradient metasurfaces. It is believed that the proposed all-dielectric metasurface will play a vital role in advanced wavefront engineering.

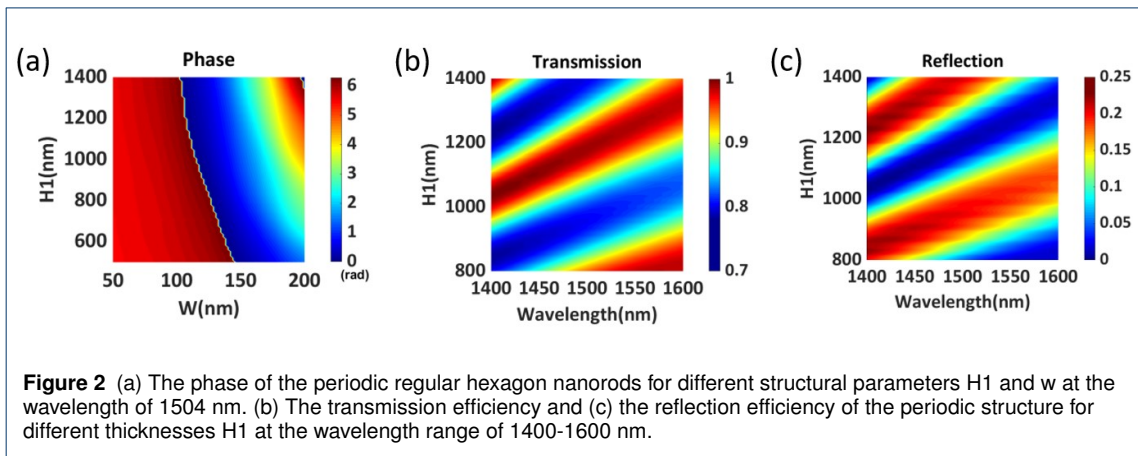
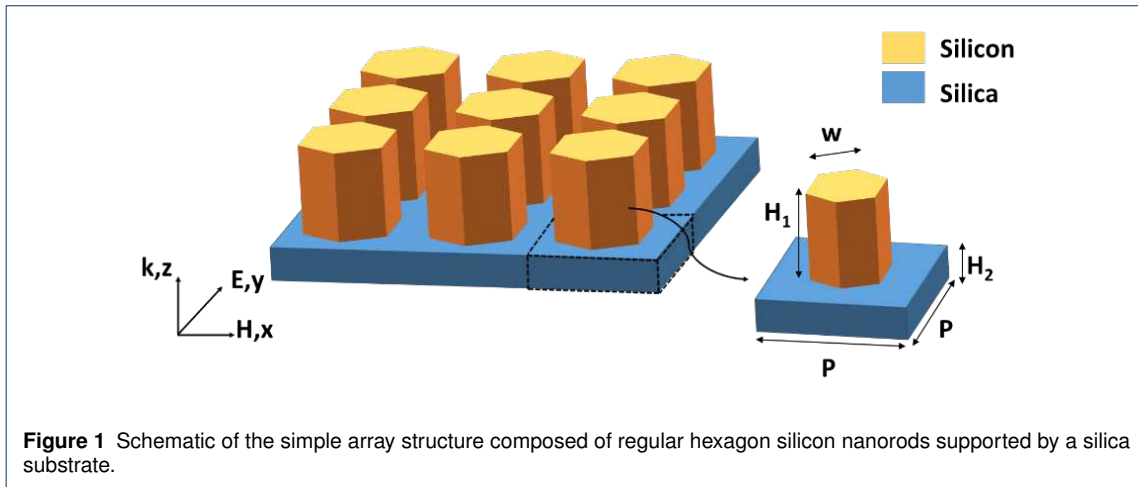
## THEORY AND SIMULATION

### Modeling and Design

For phase-gradient metasurface, the geometrical morphology and parameters play vital roles in device performance. As shown in Fig. 1, We first simulate a simple array structure composed of regular hexagon nanorods supported by a silicon substrate. The transmission efficiency and phase distributions of the simple array structure are analyzed by using the FDTD method. In the simulation, the x and y directions are set as periodic boundary conditions, and the z-direction is set as perfectly matched layers. A normally TE wave is incident from the bottom. The electric field direction of the incident light is along the y-direction, and the wavelength is 1400-1600 nm. In the numerical analysis, the refractive indexes of silicon and silicon dioxide refer to the data proposed by palik [37].

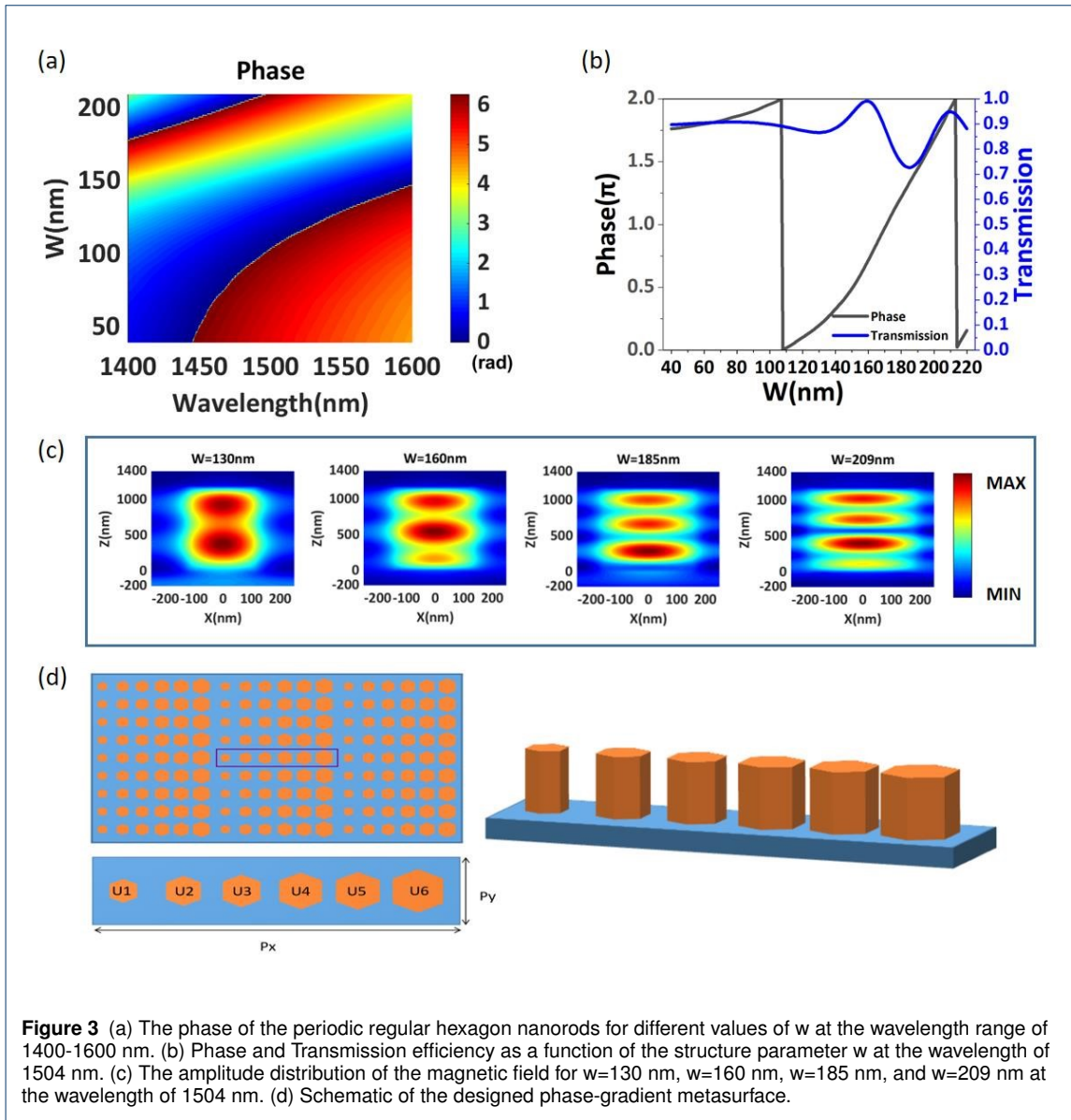
As for the proposed structure, we hope to achieve a complete  $2\pi$  phase shift by adjusting the height  $H_1$  and the side length of the regular hexagon  $w$ . When the wavelength is set as 1500 nm,  $P$  is set as 500 nm, and  $H_2$  is set as 200 nm, the phase variation with changing the lengths of  $H_1$  and  $w$  are shown in Fig. 2(a). It is clear that the phase of transmitted light varies with the side length of the regular hexagon  $w$ , but only when the height  $H_1$  is greater than 800 nm, this structure can realize a full  $2\pi$  phase shift. Furthermore, high transmission efficiency is another important factor to consider in the phase-gradient metasurface designing. Fig. 2(b) and 2(c) show the changes of transmission efficiency and reflection efficiency with the wavelength for different height  $H_1$ . The structural parameter  $w$  is set as 160 nm. As shown in Fig. 2(b), the wavelength of the peak transmission efficiency red-shifts with the height of the nanorods increasing. Obviously, the height of the nanorods has a significant effect on transmission efficiency and reflection efficiency. Here, the height  $H_1$  is set as 1200 nm. At this value, the average transmission efficiency of the simple homogeneous metasurface reaches 92.61% in the range of 1400-1600 nm, and the highest transmission efficiency is up to 99.08% at the wavelength of 1509 nm.

As shown in Fig. 3(a), when the height  $H_1$  is set as 1200 nm, the phase change is related to the side



length of  $w$  and the operating wavelength. It can be found that  $2\pi$  phase variation can be obtained when the side length of the regular hexagon  $w$  changes from 50 to 200 nm for the wavelength range of 1400-1600 nm. For further analysis, Fig. 3(b) illustrates the variation of transmission efficiency and phase with changing the regular hexagon's side length at the central wavelength of 1504 nm. As shown in Fig. 3(b), the black curve represents the transmissivity efficiency, and the blue curve represents the phase of the transmitted light. It is clear that the simple array structure can realize a full  $2\pi$  phase shift when  $w$  changes from about 110 to 210 nm, and the transmission efficiency remains at a high level

on the whole, but there are two peaks and two dips with the change of the side length. The side length for the two peaks are 165 and 209 nm, and the two dips are 130 and 185 nm, respectively. As shown in Fig. 3(c), we simulated the magnetic field distribution of the nanorods in the  $x$ - $z$  plane for different values of  $w$ . It is clear that resonance phenomena are formed in the nanorods, and different magnetic field distribution affects transmission efficiency. This resonance is similar to the Fabry-Perot resonance. It requires the nanorods to be high enough to form resonance condition for phase shift, which also explains the phenomenon shown in Fig. 2(a) [6, 38, 39]. According to the generalized Snell law, anoma-



lous transmission can be achieved if a metasurface has a  $2\pi$  phase shift ability. By adjusting the size of the nanorods so that the phase shift is evenly spaced and cover a full  $2\pi$  range, we can deflect the beam by dislocating its wavefront. Fig. 3(d) illustrates the schematic diagram of the phase-gradient metasurface. Six nanorods of different sizes array on sili-

con with  $2\pi/5$  intervals for forming a complete  $2\pi$  macrocycle. The purple box represents a complete period,  $P_x$  and  $P_y$  are 3000 nm and 500 nm, respectively. The structural parameters of each element are shown in Table 1.

### Theoretical Basis

Different from the ideal boundary, when light propagates through the metasurface, optical parameters such as polarization state, phase, and wavefront may change. We cannot explain this phenomenon with the classical Snell's law in geometric optics when electromagnetic wave propagating through such interfaces, thus giving rise to a universal generalized Snell's law [9-13]. Based on the generalized Snell law, anomalous reflection or reflection at the interface of two media comes from the horizontal phase distribution. For the two types of refractions, we can demonstrate as

$$n_r \sin \theta_r - n_i \sin \theta_i = \frac{\lambda_0}{2\pi} \frac{d\phi}{dx} \quad (1)$$

Where  $\theta_r$  and  $\theta_i$  represent the anomalous refraction angle and the incident angle, respectively,  $n_r$  usually refers to the refractive index of air, which has a magnitude of 1, while  $n_i$  refers to the refractive index of the metasurface material,  $\lambda_0$  is the operating wavelength in free space, and  $d\phi/dx$  is the phase gradient. The phase gradient metasurface needs to achieve complete near-linear  $2\pi$  phase shift over a large period to control the anomalous transmission, so the phase gradient is

$$\frac{d\phi}{dx} = \frac{2\pi}{P_x} \quad (2)$$

Where  $P_x$  is the period of the proposed metasurface along the x-axis. In this work, we only consider the normal light incidence to the interface, so  $\theta_i$  is 0, and the equation can be further simplified as

$$\sin \theta_r = \frac{\lambda_0}{2\pi} \frac{d\phi}{dx} = \frac{\lambda_0}{P_x} \quad (3)$$

As a fact, phase-gradient metasurfaces not only exist low-order anomalous transmission but also exist higher-order anomalous transmission. To solve the higher-order anomalous refraction angle, we introduce the grating equation to modify the generalized Snell's law [40-42]. The modified generalized Snell's law is

$$\sin \theta_r = m \frac{\lambda_0}{P_x} + \frac{\lambda_0}{P_x} = (m+1) \frac{\lambda_0}{P_x} \quad (4)$$

Where  $m$  represents the traditional diffraction order. Electromagnetic wave shifts from the position of the original zero-order to the position of the first order, which could be seen as the anomalous refraction angle. In addition, the period and the operating wavelength decide the total number of diffraction orders. The ratio of  $\lambda_0$  to  $P_x$  influences the desirable value of  $m$ . When  $\lambda_0/P_x$  is greater than 0.5,  $m$  could only take the value of 0, and only three diffraction orders can be obtained at this condition. The three diffraction orders are 0, -1, and 1, respectively. But when  $\lambda_0/P_x$  is less than 0.5,  $m$  could take the values of 0 and 1, and five diffraction orders can be obtained. The five diffraction orders are -2, -1, 0, 1, and 2, respectively. In the following discussion, the theory is proved by our calculated results.

To explain the characteristics of the proposed structure, we mainly calculate the efficiency and refraction angle for anomalous transmission. The total transmission efficiency and the anomalous transmission efficiency are defined as

$$T = I_{out}/I_{in} \quad (5)$$

$$\eta = I_r/I_{in} \quad (6)$$

Where  $I_{in}$  is the input intensity,  $I_{out}$  is the total transmission intensity, and  $I_r$  is the transmitted intensity along the anomalous refraction angle.

## Results and discussion

Table 1 shows the structural parameters of each element. We investigate the phase distribution and intensity of the transmission light. To facilitate analysis, we set the origin of the coordinates at the center of the super cell. We simulate the phase distribution of the transmission light at the wavelength range of 1400-1600 nm. Through the super cell, it is evident that the proposed structure can realize a full  $2\pi$  phase shift in the range of 1400-1600 nm. To make it clear, Fig. 4(b) shows the phase shift curve at the central wavelength of 1504 nm. As shown in Fig. 4(b), we can see that the phase shift shows a linear trend and are very smooth. According to the generalized Snell's law, the better the linearity of the phase shift, the flatter the equip phase

plane of the transmitted light will be. We simulated the total transmission and reflectance of the proposed metasurface for the range of 1400-1600 nm, and the results are shown in Fig. 4(c). By observing the curve, we can see that the total transmission remains a high efficiency. It exceeds 60% in the whole operating wavelength range. At the center wavelength of 1504 nm, the total transmission efficiency achieves 97.9% with a reflection efficiency of 2.0%. The result shows that the absorption rate is much less than 0.1% because the imaginary part of the permittivity of silicon in the near-infrared wavelength is very small. So the absorption rate can be negligible. Transmission efficiency and reflection efficiency have opposite trends with the wavelength, and the loss of the structure mainly comes from reflection. It is clear that the proposed phase-gradient metasurface can realize a complete near-linear  $2\pi$  phase shift and simultaneously maintain higher transmission efficiency at the range of 1400-1600 nm.

As shown in Fig. 5(a), we also calculate the desired anomalous transmission efficiency of the phase-gradient metasurface in the whole operating wavelength range and normalize it to the energy of incident light. Comparing Fig. 4(c) and Fig. 5(c), we can see that the trend of the total transmission efficiency and anomalous transmission efficiency with wavelength is consistent. From Fig. 5(a), we can see that the lowest anomalous transmission is 22.3% in the range of 1400-1600 nm. The desired anomalous transmission efficiency exceeds 80% of the wavelength range of 1499-1532 and 1549-1600 nm. It includes the optical communication wavelength of 1550 nm. What's more remarkable is that the anomalous transmission efficiency is as high as 96.1% at the central wavelength of 1504 nm. As far as we know, the value is far higher than most reported phase-gradient metasurfaces at present [2-16,22-34].

Fig. 5(b) shows the relationship between the far-field transmission efficiency and the anomalous refraction angle for the wavelength of 1504 nm. It can be seen that the far-field energy of the transmitted light is mainly concentrated at the angle of  $30.09^\circ$ , and only weak energy is distributed in the other two

angles. For easy observation, Fig. 5(c) shows the phase distribution of the metasurface configuration at the center wavelength. From Fig. 5(b), we can see that the transmitted light is obviously refracted, and the wavefront is relatively flat. By substituting the working wavelength and the period of the structure into Eq.(3), the calculated angle of the anomalous transmission  $\theta_r$  is  $30.088^\circ$ , which is very close to our simulation results. To verify the relationship of the number of diffraction orders and the ratio of the wavelength to the period, we take  $\lambda_0/P_x$  as the critical value of 0.5 and select five different wavelengths to perform theoretical calculations and FDTD simulations. The results are shown in Table 2. Obviously, the simulation results are highly consistent with the calculated results.

According to calculation and Simulation Angles for the proposed structure shown in Table 2, when  $\lambda_0/P_x$  is greater than 0.5, there is only diffraction order 0 and diffraction order 1, but there is no diffraction order 2. When  $\lambda_0/P_x$  is less than 0.5, diffraction orders 0, 1, and 2 are obtained in the simulation. This result is in complete agreement with the theoretical analysis described above and thus fully confirms the reliability of the generalized Snell's law combined with the grating theory.

It can be seen from Eq. (3) that the diffraction angle of anomalous transmission light is affected by  $\lambda_0/P_x$ , so we try to change the magnitude of  $P_x$  to obtain different anomalous refraction angles. An effective method to realize different anomalous refraction angle is to change the number of elements in the period. Therefore, we further designed the phase gradient metasurfaces with multiple sets. The elements of the metasurface in one periodicity is changing from three to nine. We select the working wavelength with the highest anomalous transmission efficiency for each group of metasurface and observe the phase distribution of the transmitted light. The simulation results are plotted in Fig. 6(a)-(f). The anomalous transmission angle increases from  $18.98^\circ$  to  $68.03^\circ$  with the elements in one unit cell reducing from nine to three. It can be seen from Figs. 6(a)-(f) that the phase-gradient metasurfaces with different elements can realize near-linear phase distributions, and the wavefront of the transmitted light is relatively smooth. We carried out the far-field analysis

**Table 1** The side length of the regular hexagon nanorods.

Unit cell	$U_1(0^\circ)$	$U_2(72^\circ)$	$U_3(144^\circ)$	$U_4(216^\circ)$	$U_5(288^\circ)$	$U_6(360^\circ)$
$w(\text{nm})$	113	142	154	176	179	208

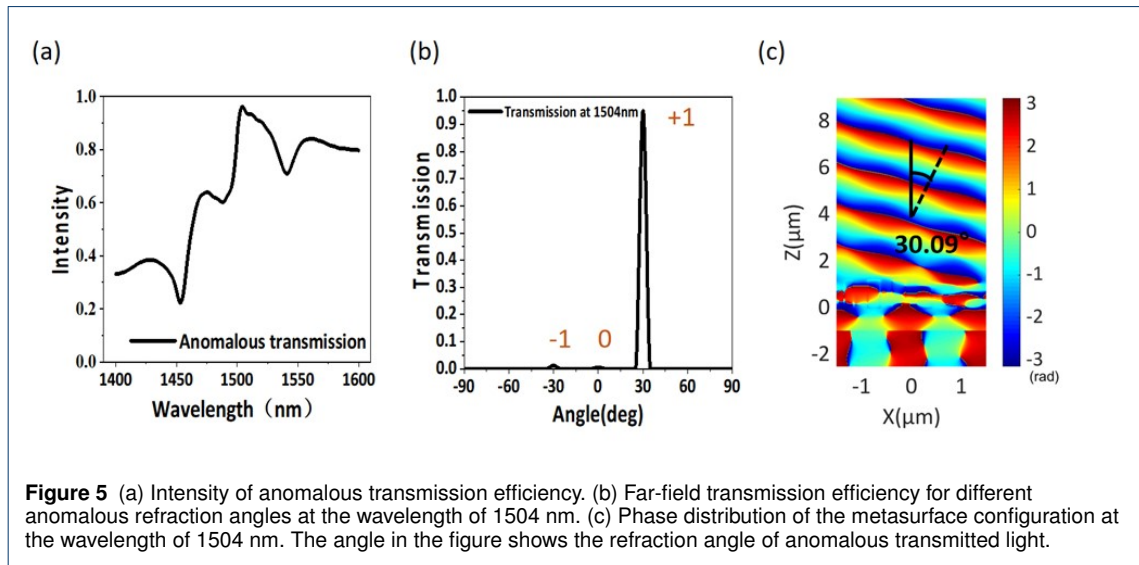
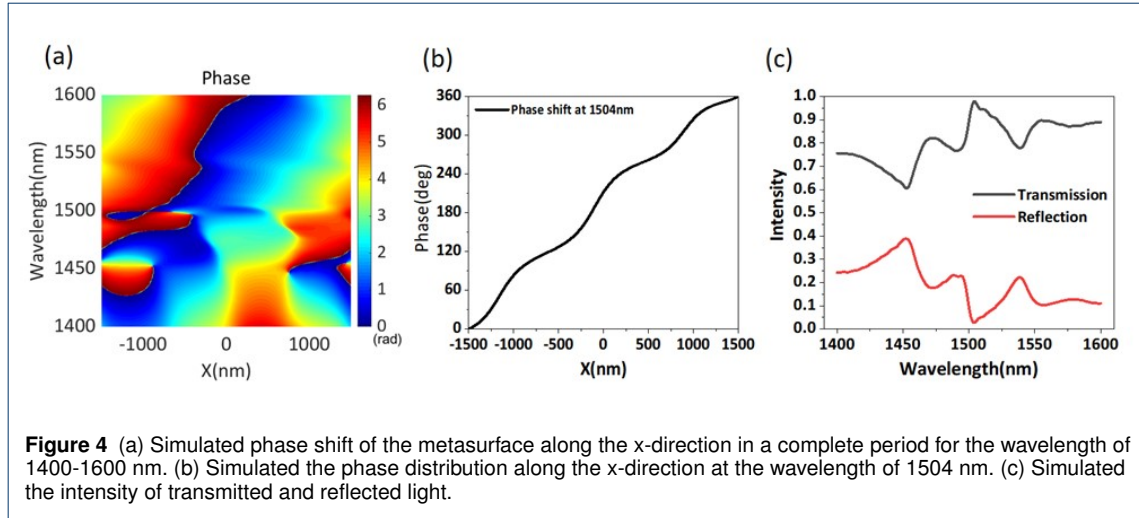
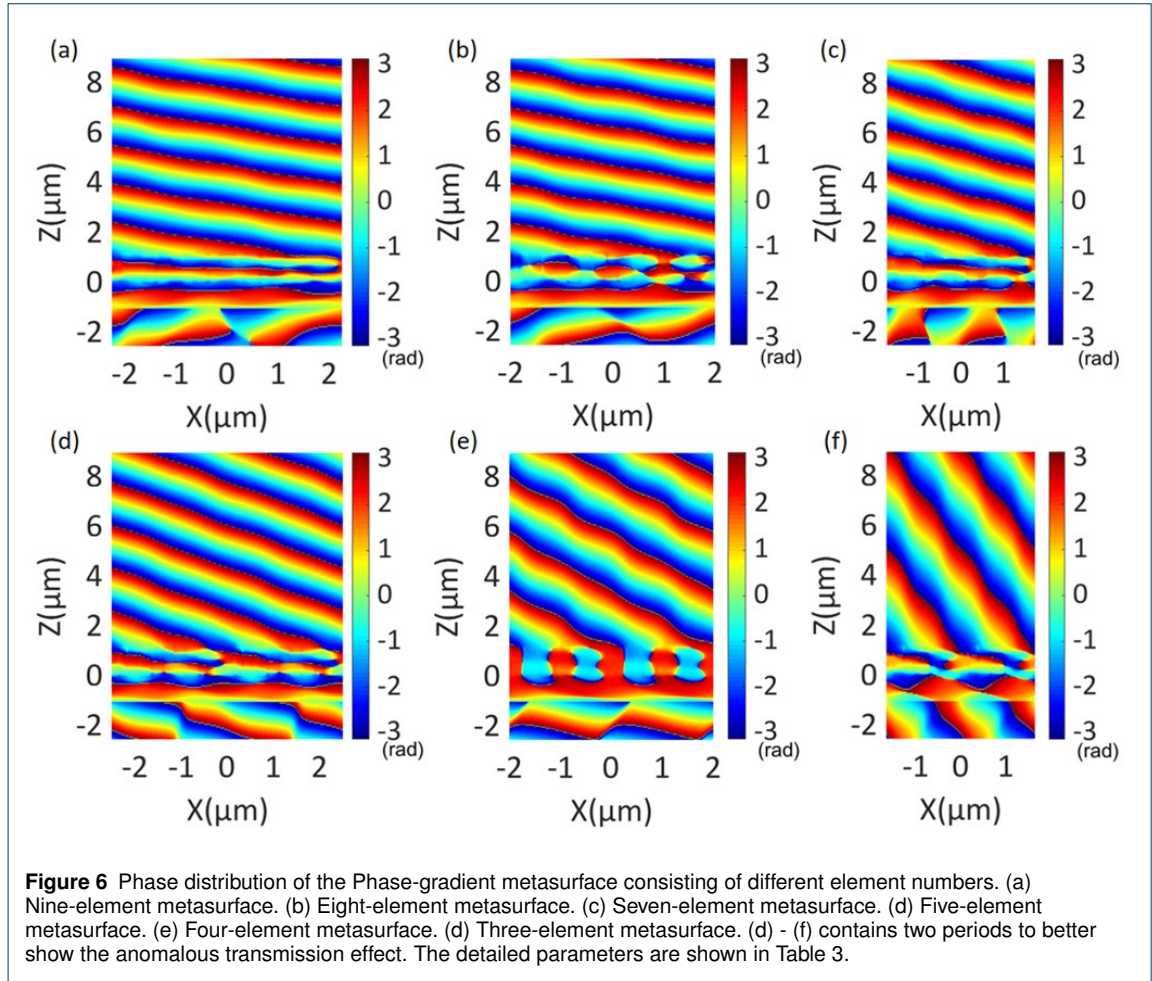


**Table 2** Calculation and Simulation Angles for +1 Order and +2 Order.

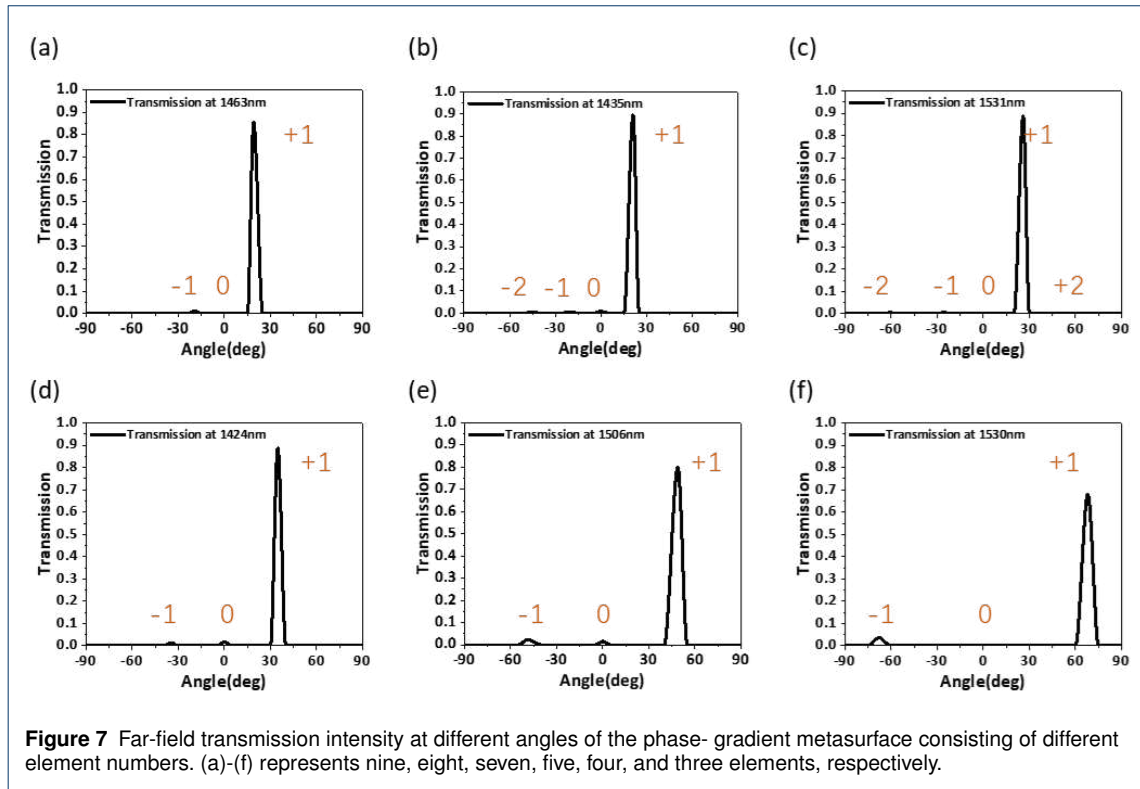
$\lambda(\text{nm})$	1495	1499	1504	1508	1510
$\lambda/P$	0.4983	0.4997	0.5013	0.5027	0.5033
Calculation 1 order	29.8876	29.9802	30.0860	30.1788	30.2186
angle(deg) 2 order	85.2739	88.0151	—	—	—
Simulation 1 order	29.8898	29.9779	30.0883	30.1766	30.2208
angle(deg) 2 order	85.3205	87.9077	—	—	—



of the above configurations and plotted the energy distribution of transmitted light along each diffraction angle, as shown in Figs. 7(a)-(f). We can obtain more than 80% abnormal transmission efficiency from  $18.98^\circ$  to  $48.86^\circ$ . The structural parameters of each element and detailed numerical results are listed in Table 3. In our optimizing process, the side length of the regular hexagon  $w$  and the period  $P$  are the main optimization parameters.

According to the generalized Snell's Law, in order to design a larger anomalous refraction angle  $\theta_r$ , the ratio of working wavelength  $\lambda$  to structural period  $P_x$  should be increased. As shown in Fig. 8(a), we plotted the phase variation of the transmitted light

along the x-direction for the wavelengths of 1400-1600 nm. We select four wavelength points 1450 nm, 1500 nm, central working wavelength 1530 nm, and 1550 nm for plotting the phase shift curves shown in Fig. 8(b). It is clear that the all-dielectric metasurface can be realized a full  $2\pi$  phase shift for the wavelength points. From Fig. 8(b), we can see that the phase variation shows a linear trend along the x-direction. We calculate the total transmission efficiency and the desired anomalous transmission efficiency of the structure in the working band, respectively, and the results are shown in Fig. 8(c). It can be observed that the total transmission efficiency is lower than before. However, the anoma-

**Table 3** The side length of the regular hexagon nanorods.

$N$	$U_1$	$U_2$	$U_3$	$U_4$	$U_5$	$U_6$	$U_7$	$U_8$	$U_9$	$\eta$	$P$	$\lambda$	$\theta$
3	0.131	0.181	0.203	—	—	—	—	—	—	67.8%	1.65	1.530	68.03°
4	0.080	0.153	0.173	0.196	—	—	—	—	—	80.1%	2.0	1.506	48.86°
5	0.103	0.146	0.153	0.166	0.193	—	—	—	—	88.6%	2.5	1.424	34.73°
6	0.113	0.142	0.154	0.176	0.179	0.208	—	—	—	96.1%	3.0	1.504	30.09°
7	0.119	0.139	0.153	0.171	0.173	0.193	0.214	—	—	88.6%	3.5	1.531	25.94°
8	0.089	0.138	0.150	0.157	0.165	0.168	0.185	0.197	—	89.4%	4.0	1.435	21.03°
9	0.114	0.145	0.149	0.160	0.164	0.173	0.182	0.192	0.202	85.7%	4.5	1.463	18.98°

lous transmission efficiency can remain above 60% in the broadband range from 1506 nm to 1555 nm and reaches 67.9% at the wavelength of 1530 nm. The anomalous refraction angle within the bandwidth can reach 70.47°. The phase distribution of transmitted light and energy distributions at different anomalous refraction angles are shown in Fig. 6 (f) and Fig. 7(f), respectively. By observing the distribution of the electric field, we can clearly see that the equilateral phase plane of the transmitted light is very flat. The transmitted light has very little energy emitting at 0° and symmetric -68.03°, but the ma-

jority of transmitted light is concentrated at 68.03°. The anomalous transmission performance of the all-dielectric phase gradient metasurface designed by us is better than that of most of the metasurface structures proposed before, and the anomalous transmission efficiency can reach more than 60% within the range of anomalous refraction angle from 0° to 70°. Based on the above analysis, the anomalous refraction angle of about 30° is the most reasonable. At this anomalous refraction angle, the highest anomalous transmission efficiency can be achieved, and the

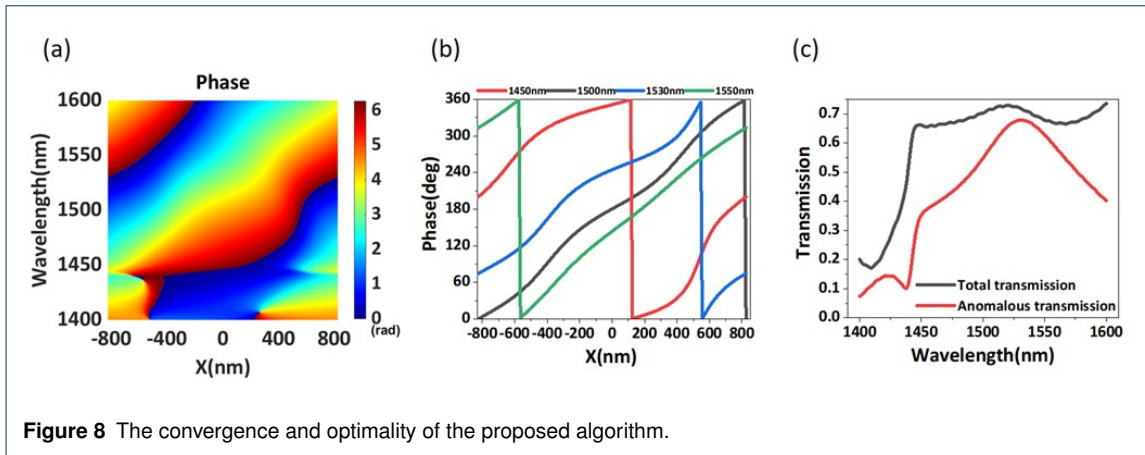


**Figure 8** The convergence and optimality of the proposed algorithm.

anomalous refraction angle can be guaranteed to be large enough.

## Conclusions

In summary, we design and simulate an all-dielectric phase-gradient metasurface for performing high-efficiency anomalous transmission in the near-infrared region. The metasurface consists of regular hexagonal silicon nanorods arranged on a silica substrate. The FDTD method is used to simulate the transmission efficiency and anomalous refraction angle of the transmitted light. The results show that the metasurface can realize a complete  $2\pi$  phase shift in the wavelength range of 1400–1600 nm. At the centre wavelength of 1504 nm, the desired anomalous transmission efficiency reaches 96.1% with an anomalous refraction angle of  $30.11^\circ$ . The anomalous transmission efficiency exceeds 80% in the range of 1499–1532 nm, which makes our design more flexible. We also design multiple sets of phase-gradient metasurfaces by changing the number of elements in one unit cell and adjusting the period of the metasurface. The optimized results show that we can adjust the refraction angle in the range of  $18.98^\circ$ – $70.47^\circ$ . When the anomalous refraction angle is less than  $48.86^\circ$ , more than 80% of the anomalous transmission efficiency can be obtained. Such an all-dielectric metasurface will easily find applications in integrated optical devices.

## Funding

National Natural Science Foundation of China (61805051); Natural Science Foundation of Guangxi Province (2018JJB170035, 2018AD19071, 2019GXNSFFA245002); Dean Project of Guangxi Key Laboratory of Wireless Broadband Communication and Signal Processing (GXKL06190118, GXKL06160102).

## Abbreviations

SP: Surface plasma; FDTD: Finite difference time domain

## Competing interests

The authors declare that they have no competing interests.

## Authors' contributions

TW, ZL carried out the simulation and wrote the paper. HZ, ZY, and DY created the figures. YW supervised the whole work. All the authors reviewed the manuscript. All authors read and approved the final manuscript.

## Author details

<sup>1</sup>Key Laboratory of Optoelectronic Devices and Systems of Ministry of Education and Guangdong Province, Shenzhen University, Shenzhen 518060, China. <sup>2</sup>Guangxi Key Laboratory of Wireless Broadband Communication and Signal Processing, School of Information and Communication, Guilin University of Electronic Technology, Guilin 541004, China. <sup>3</sup>Key Laboratory of Optoelectronic Devices and Systems of Ministry of Education and Guangdong Province, College of Optoelectronic Engineering, Shenzhen University, Shenzhen 518060, China.

## References

- Zhang L., Mei S.T., Huang K., Qiu C.W.: Advances in full control of electromagnetic waves with metasurfaces. *Adv. Opt. Mater.* **5**, 818–833 (2016)
- Wang Y., Liu Y., Li J., Liu C., Yu Z. Y., Ye H., Yu L.: Broadband Ultrathin Transmission Quarter Waveplate with Rectangular Hole Array Based on Plasmonic Resonances. *Nanoscale Res. Lett.* **14**, 384 (2019)
- Meng C., Tang S.W., Ding F., Bozhevolnyi S. I.: Optical Gap-Surface Plasmon Metasurfaces for Spin-Controlled Surface Plasmon Excitation and Anomalous Beam Steering. *ACS Photon.* **7**, 1849–1856 (2020)

4. Shalaev M.I., Sun J.B., Tsukernik A., Pandey A., Nikolskiy K., Litchinister N.M.: High-Efficiency All-Dielectric Metasurfaces for Ultracompact Beam Manipulation in Transmission Mode. *Nano Lett.* **15**, 6261–6266 (2015)
5. Zhao W.C., Wang K., Hong X.M., Wang B.X., Han X.B., Long H., Wang B., Lu P.X.: Chirality-selected second-harmonic holography with phase and binary amplitude manipulation. *Nanoscale* **12**, 13330–13337 (2020)
6. Zhou Z.P., Li J.T., Su R.B., Yao B.M., Fang H.L., Li K.Z., Zhou L.D., Liu J., Stellinga D., Reardon C.P., Krauss T.F., Wang X.H.: Efficient Silicon Metasurfaces for Visible Light. *ACS Photon.* **4**, 544–551 (2017)
7. Lin B.Q., Guo J.X., Lv L.T., Liu Z., Ji X., Wu J.: An ultra-Wideband Reflective Phase Gradient Metasurface Using Pancharatnam-Berry Phase. *IEEE Access* **7**, 13317–13325 (2019)
8. Fang N., Lee H., Sun C., Zhang X.: Sub-diffraction-limited optical imaging with a silver superlens. *Science* **308**, 534–537 (2005)
9. Xu T., Wang C.T., Du C.L., Luo X.G.: Plasmonic beam deflector. *Opt. Express* **16**, 4753–4759 (2008)
10. Shi J.H., Fang X., Rogers E.T.F., Plum E., Macdonald K.F., Zheludev N.I.: Coherent control of Snell's law at metasurfaces. *Opt. Express* **22**, 21051–21060 (2014)
11. Zhang J., Zhao X.H., Zheng Y.L., Chen X.F.: Generalized nonlinear Snell's law at  $\chi(2)$  modulated nonlinear metasurfaces: anomalous nonlinear refraction and reflection. *Opt. Lett.* **44**, 431–434 (2019)
12. Larouche S., Smith D.R.: Reconciliation of generalized refraction with diffraction theory. *Opt. Lett.* **37**, 2391–2393 (2012)
13. Yu N.F., Genevet P., Kats M.A., Aieta F., Tetienne J.P., Capasso F., Gaburro Z.: Light Propagation with Phase Discontinuities: Generalized Laws of Reflection and Refraction. *Science* **334**, 333–337 (2011)
14. Fahad A.K., Ruan C.J., Ali S.A.K.M., Nazir R., Haq T.U., Ullah S., He W.L.: Triple-wide-band Ultra-thin Metasheet for transmission polarization conversion. *Sci. Rep.* **10**, 8810 (2020)
15. Yu Y.Z., Xiao F.J., He C., Jin R.H., Zhu W.R.: Double-arrow metasurface for dual-band and dual-mode polarization conversion. *Opt. Express* **28**, 11797–11805 (2020)
16. Fei P., Vandenbosch G.A.E., Guo W.H., Wen X., Xiong D., Hu W., Zheng Q., Chen X.: Versatile Cross-Polarization Conversion Chiral Metasurface for Linear and Circular Polarizations. *Adv. Opt. Mater.* **8**, 2000194 (2020)
17. Ha Y.L., Guo Y.H., Pu M.B., Li X., Ma X.K., Luo X.G.: A Tunable Metasurface Deflector Based on MIM Waveguide Filled with Phase-Change Material. *Plasmonics* **14**, 1735–1741 (2019)
18. Su X.Q., Ouyang C.M., Xu N.N., Cao W., Wei X., Song G.F., Gu J.Q., Tian Z., O'Hara J.F., Han J.G., Zhang W.L.: Active metasurface terahertz deflector with phase discontinuities. *Opt. Express* **23**, 27152–27158 (2015)
19. Li N.X., Fu Y.H., Dong Y., Hu T., Xu Z.J., Zhong Q.Z., Li D.D., Lai K.H., Zhu S.Y., Lin Q.Y., Gu Y.D., Singh N.: Large-area pixelated metasurface beam deflector on a 12-inch glass wafer for random point generation. *Nanophotonics* **8**, 1855–1864 (2019)
20. Zhang Q., Li M.Z., Liao T.D., Cui X.D.: Design of beam deflector, splitters, wave plates and metalens using photonic elements with dielectric metasurface. *Opt. Express* **411**, 93–100 (2018)
21. Sun S.L., He Q., Xiao S.Y., Xu Q., Li X., Zhou L.: Gradient-index meta-surfaces as a bridge linking propagating waves and surface waves. *Nat. Mater.* **11**, 426–431 (2012)
22. Tavakol M.R., Khabasi A.: Reconfigurable Meta-Coupler Employing Hybrid Metal-Graphene Metasurfaces. *Sci. Rep.* **10**, 7684 (2020)
23. Yin L.Z., Huang T.J., Han F.Y., Liu J.Y., Wang D., Liu P.K.: High-efficiency terahertz spin-decoupled meta-coupler for spoof surface plasmon excitation and beam steering. *Opt. Express* **27**, 18928–18939 (2019)
24. Zhao R.Z., Sain B., Wei Q.S., Tang C.C., Li X.W., Weiss T., Huang L.L., Wang Y.T., Zentgraf T.: Multichannel vectorial holographic display and encryption. *Light: Sci. Appl.* **7**, 95 (2018)
25. Wang B., Dong F.L., Li Q.T., Yang D., Sun C.W., Chen J.J., Song Z.W., Xu L.H., Chu W.G., Xiao Y.F.: Visible-Frequency Dielectric Metasurfaces for Multiwavelength Achromatic and Highly Dispersive Holograms. *Nano Lett.* **16**, 5235–5240 (2016)
26. Jin L., Dong Z.G., Mei S.T., Yu Y.F., Wei Z., Pan Z.Y., Rezaei S.D., Li X.P., Kuznetsov A.I., Kivshar Y.S.: Noninterleaved Metasurface for  $(2^{(6)}-1)$  Spin- and Wavelength-Encoded Holograms. *Nano Lett.* **18**, 8016–8024 (2018)
27. Sun J.B., Wang X., Xu T.B.Y., Kudyshev Z.A., Cartwright A.N., Litchinitser N.M.: Spinning Light on the Nanoscale. *Nano Lett.* **14**, 2726–2729 (2014)
28. Bao Y.J., Ni J.C., Qiu C.W.: A Minimalist Single-Layer Metasurface for Arbitrary and Full Control of Vector Vortex Beams. *Adv. Mater.* **32**, 1905659 (2019)
29. Maguid E., Yulevich I., Yannai M., Kleiner V., Brongersma M.L., Hasman E.: Multifunctional interleaved geometric-phase dielectric metasurfaces. *Light: Sci. Appl.* **6**, e17027 (2017)
30. Huang C., Yang J.N., Wu X.Y., Song J.K., Pu M.B., Wang C.T., Luo X.G.: Reconfigurable metasurface cloak for dynamical electromagnetic illusions. *ACS Photon.* **5**, 1717–1725 (2018)
31. Yu N.F., Capasso F.: Flat optics with designer metasurfaces. *Nat. Mater.* **13**, 139–150 (2014)
32. Nalik G.V., Shalaev V.M., Boltasseva A.: Alternative Plasmonic Materials: Beyond Gold and Silver. *Adv. Mater.* **25**, 3264–3294 (2013)
33. Zhu W.R., Xiao F.J., Kang M., Premaratne M.: Coherent perfect absorption in an all-dielectric metasurface. *Appl. Phys. Lett.* **108**, 121901 (2016)
34. Proust J., Bedu F., Gallas B., Ozerov I., Bonod N.: All-Dielectric Colored Metasurfaces with Silicon Mie Resonators. *ACS Nano* **10**, 7761–7767 (2016)
35. Yang L., Wu D., Liu Y.M., Liu C., Xu Z.H., Li H., Yu Z.Y., Yu L., Ye H.: High-efficiency all-dielectric transmission metasurface for linearly polarized light in the visible region. *Photonics Res.* **6**, 517–524 (2018)
36. Liu C., Chen L., Wu T.S., Liu Y.M., Li J., Wang Y., Yu Z.Y., Ye H., Yu L.: All-dielectric three-element transmissive Huygens' metasurface performing anomalous refraction. *Photonics Res.* **7**, 1501–1510 (2019)
37. Palik E.: *Handbook of Optical Constants of Solids*. pp. 77–135. USA: Academic, Boston (1991)
38. Lv Y.H., Ding X., Wang B.Z.: Dual-Wideband High-Gain Fabry-Perot Cavity Antenna. *IEEE Access* **8**, 4754–4760 (2020)
39. Wu P.H., Wang Y.Y., Yi Z., Huang Z., Xu Z.S., Jiang P.P.: A Near-Infrared Multi-Band Perfect Absorber Based on 1D Gold

- Grating Fabry-Perot Structure. *IEEE Access* **8**, 72742–72748 (2020)
40. Huang L.L., Chen X.Z., Muhlenbernd H., Li G.X., Bai B.F., Tan Q.F., JinG.F., Zentgraf T., Zhang S.: Dispersionless Phase Discontinuities for Controlling Light Propagation. *Nano Lett.* **12**, 5750–5755 (2012)
  41. Gao S., Yue W., Park C.S., Lee S.S., Kim E.S., Choi D.Y.: Aluminum Plasmonic Metasurface Enabling a Wavelength-Insensitive Phase Gradient for Linearly Polarized Visible light. *ACS Photon.* **4**, 322–328 (2017)
  42. Zhang L., Hao J.M., Qiu M., Zouhdi S., Yang J.K.W., Qiu C.W.: Anomalous behavior of nearly-entire visible band manipulated with degenerated image dipole array. *Nanoscale* **6**, 12303–12309 (2014)

# Figures

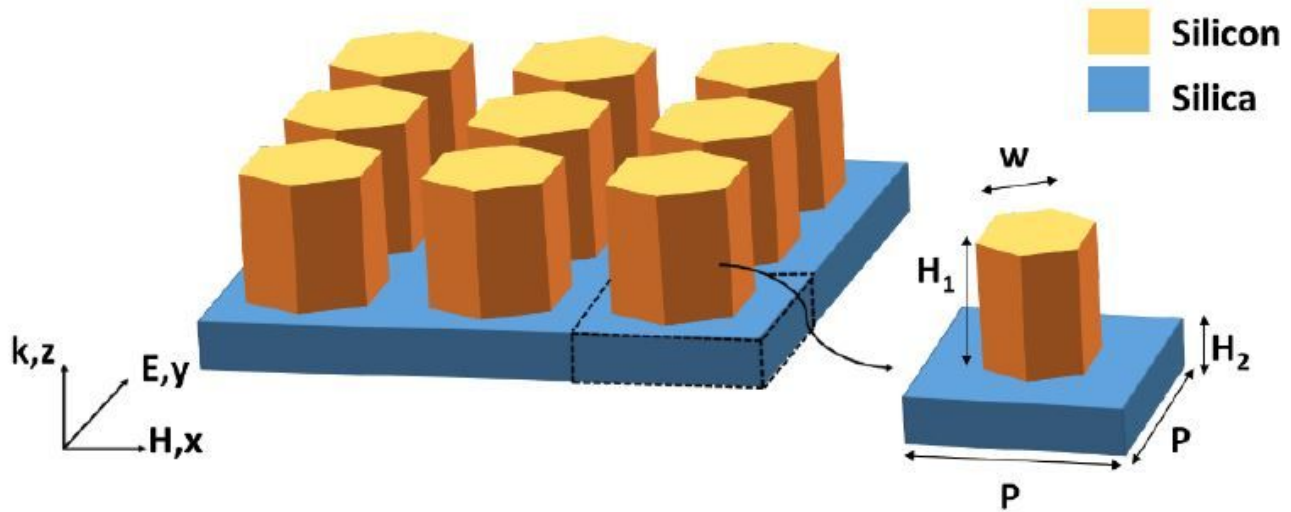


Figure 1

Schematic of the simple array structure composed of regular hexagon silicon nanorods supported by a silica substrate.

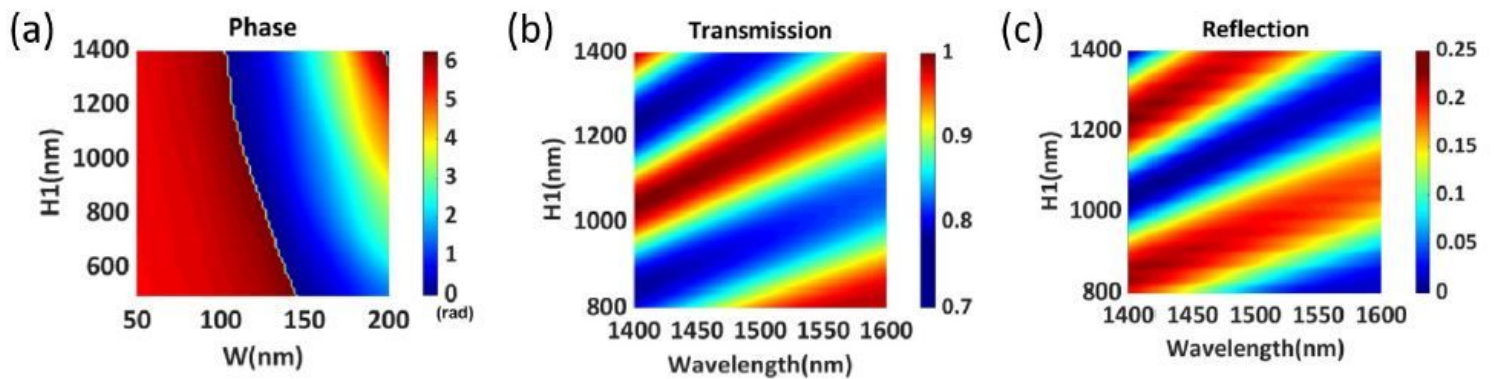
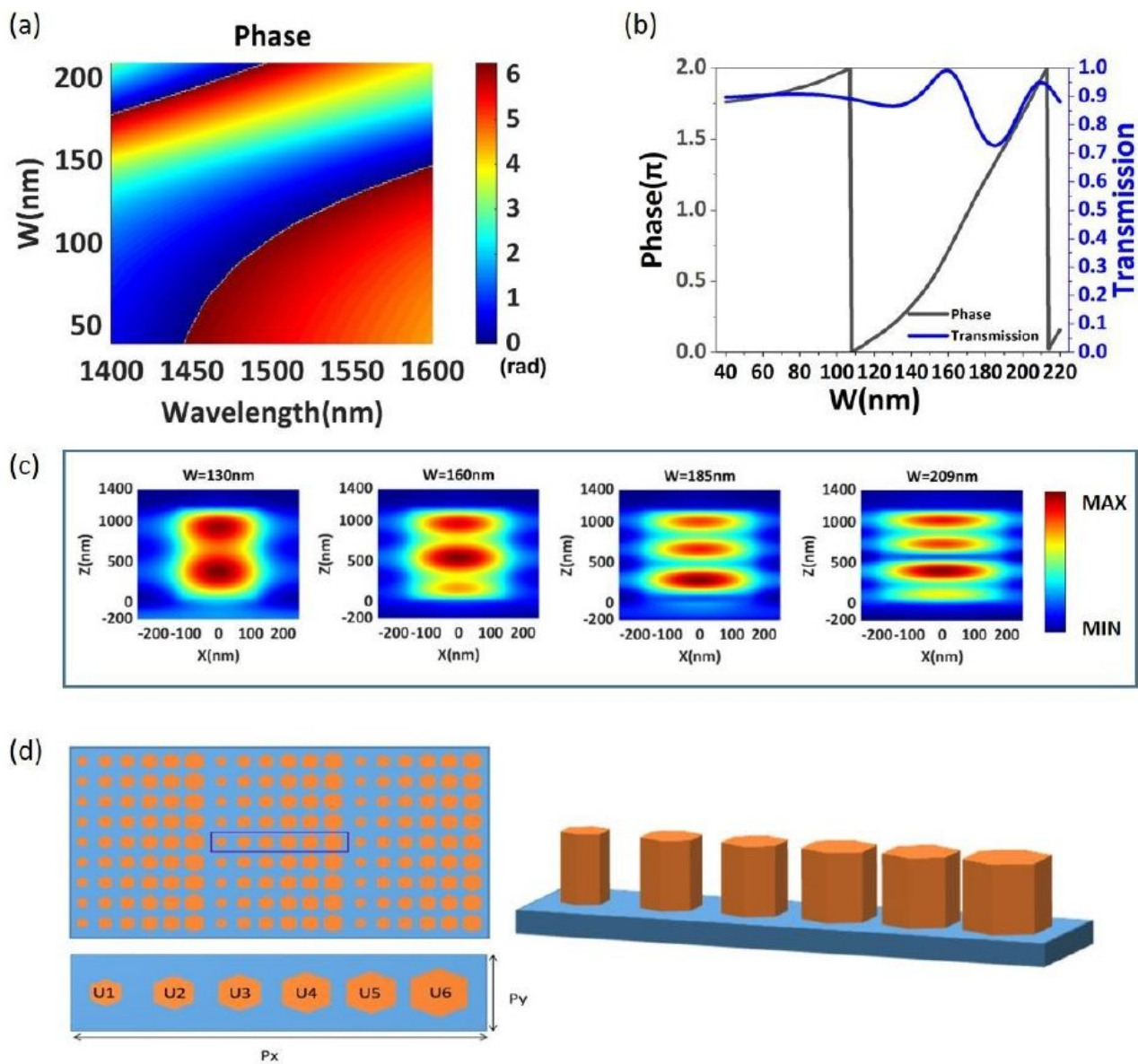


Figure 2

(a) The phase of the periodic regular hexagon nanorods for different structural parameters  $H_1$  and  $w$  at the wavelength of 1504 nm. (b) The transmission efficiency and (c) the reflection efficiency of the periodic structure for different thicknesses  $H_1$  at the wavelength range of 1400-1600 nm.



**Figure 3**

(a) The phase of the periodic regular hexagon nanorods for different values of  $w$  at the wavelength range of 1400-1600 nm. (b) Phase and Transmission efficiency as a function of the structure parameter  $w$  at the wavelength of 1504 nm. (c) The amplitude distribution of the magnetic field for  $w=130$  nm,  $w=160$  nm,  $w=185$  nm, and  $w=209$  nm at the wavelength of 1504 nm. (d) Schematic of the designed phase-gradient metasurface.

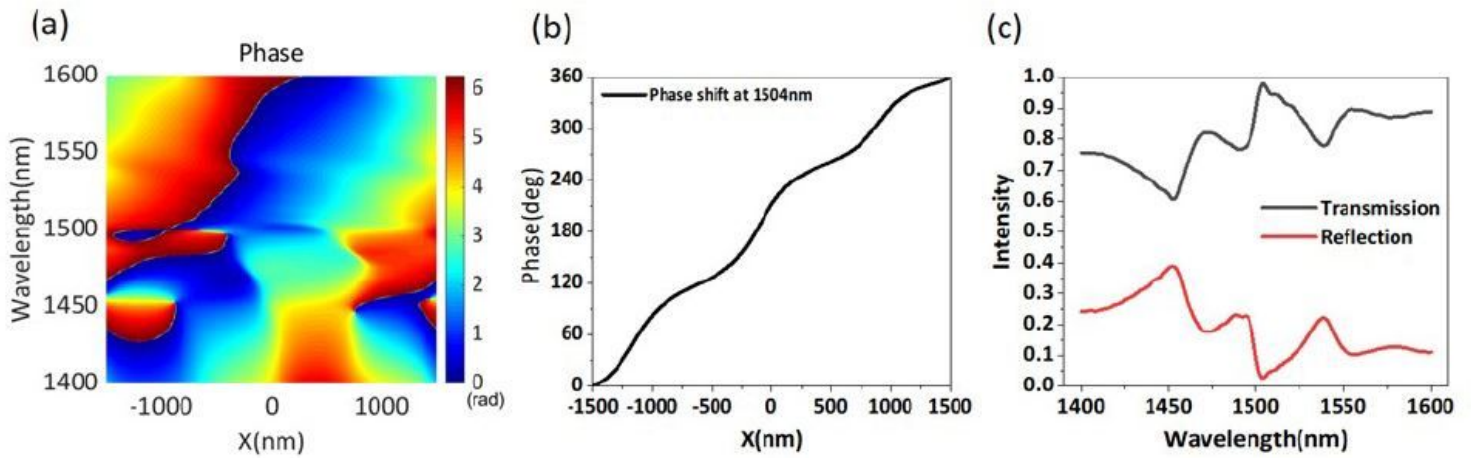


**Figure 4**

(a) Simulated phase shift of the metasurface along the x-direction in a complete period for the wavelength of 1400-1600 nm. (b) Simulated the phase distribution along the x-direction at the wavelength of 1504 nm. (c) Simulated the intensity of transmitted and reflected light.

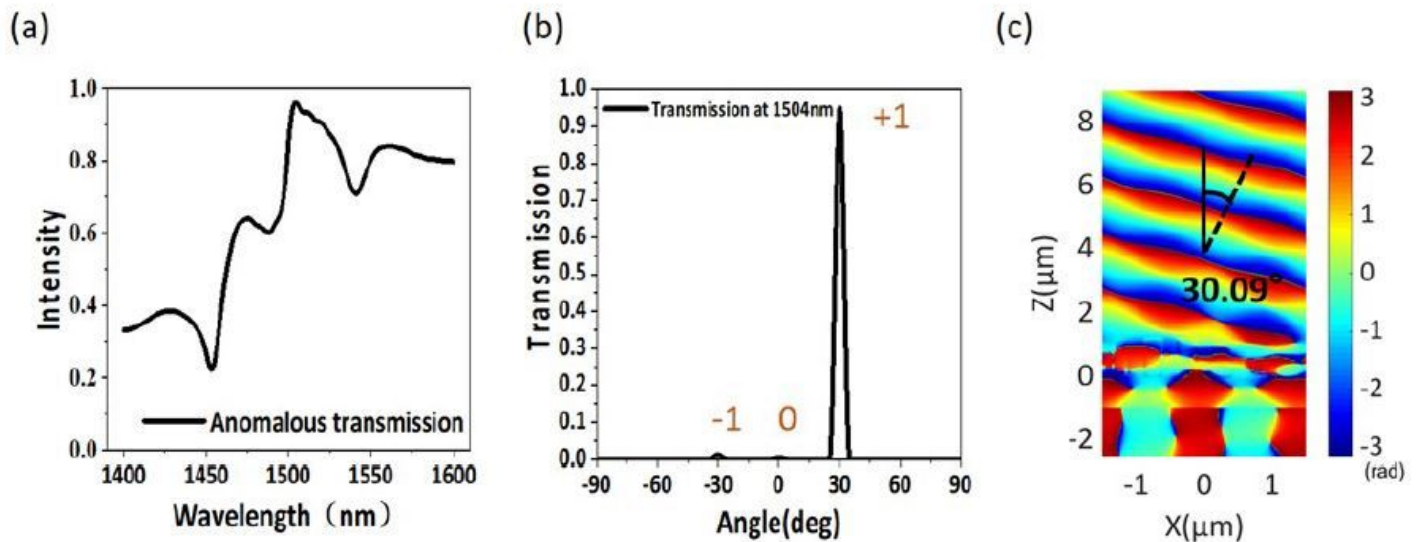


**Figure 5**

(a) Intensity of anomalous transmission efficiency. (b) Far-field transmission efficiency for different anomalous refraction angles at the wavelength of 1504 nm. (c) Phase distribution of the metasurface configuration at the wavelength of 1504 nm. The angle in the figure shows the refraction angle of anomalous transmitted light.

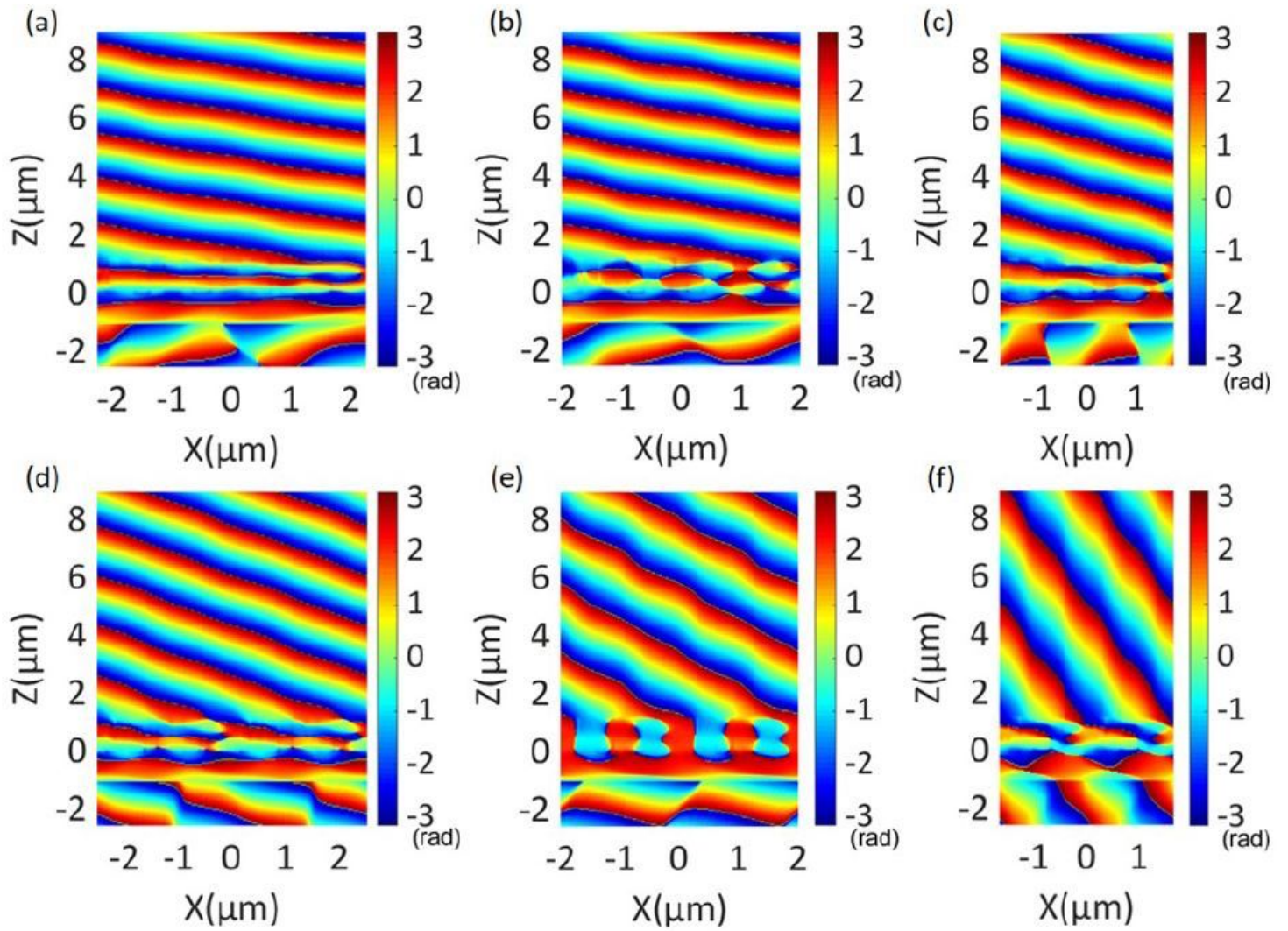


**Figure 6**

Phase distribution of the Phase-gradient metasurface consisting of different element numbers. (a) Nine-element metasurface. (b) Eight-element metasurface. (c) Seven-element metasurface. (d) Five-element metasurface. (e) Four-element metasurface. (d) - (f) contains two periods to better show the anomalous transmission effect. The detailed parameters are shown in Table 3.

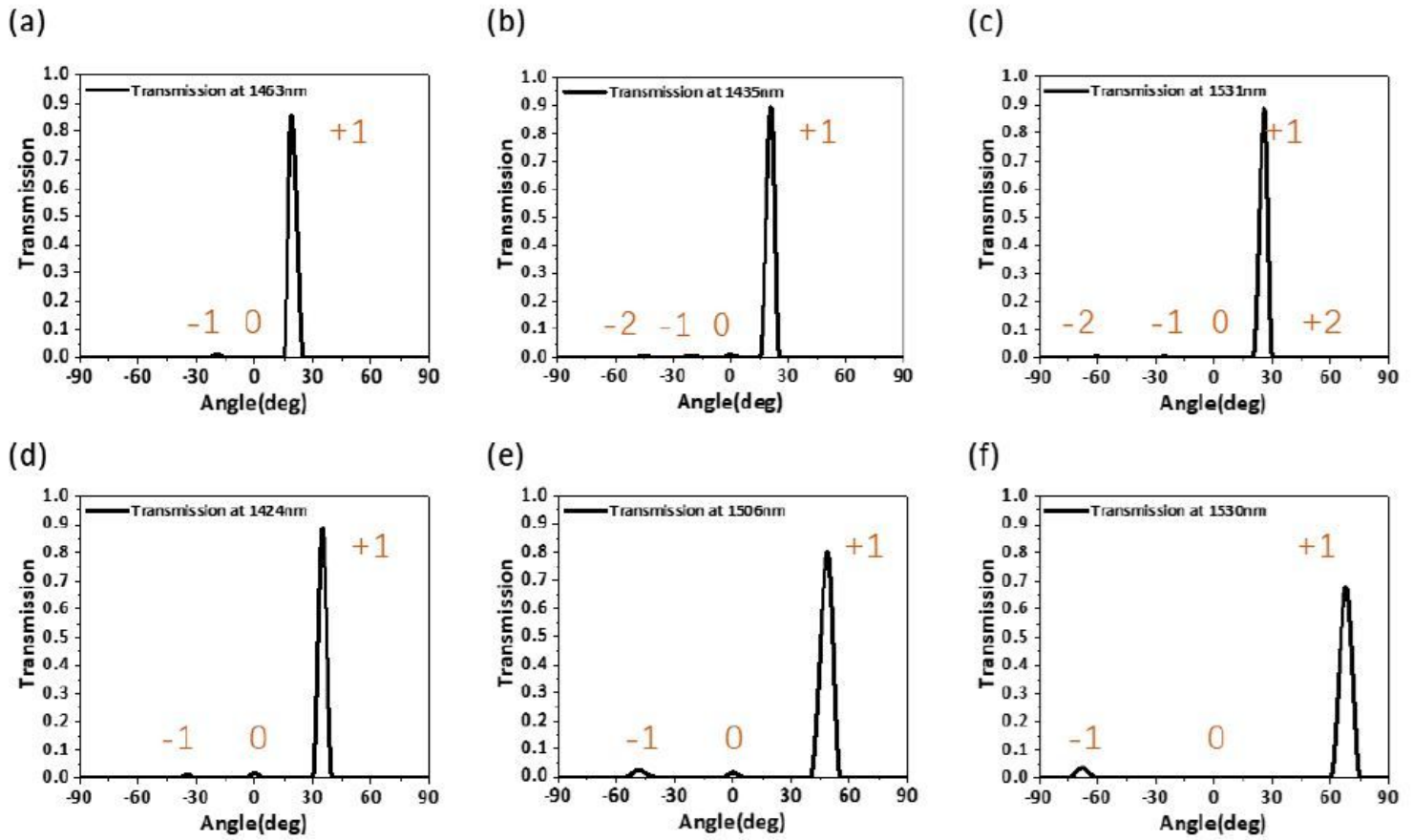


Figure 7

Far-field transmission intensity at different angles of the phase- gradient metasurface consisting of different element numbers. (a)-(f) represents nine, eight, seven, five, four, and three elements, respectively.

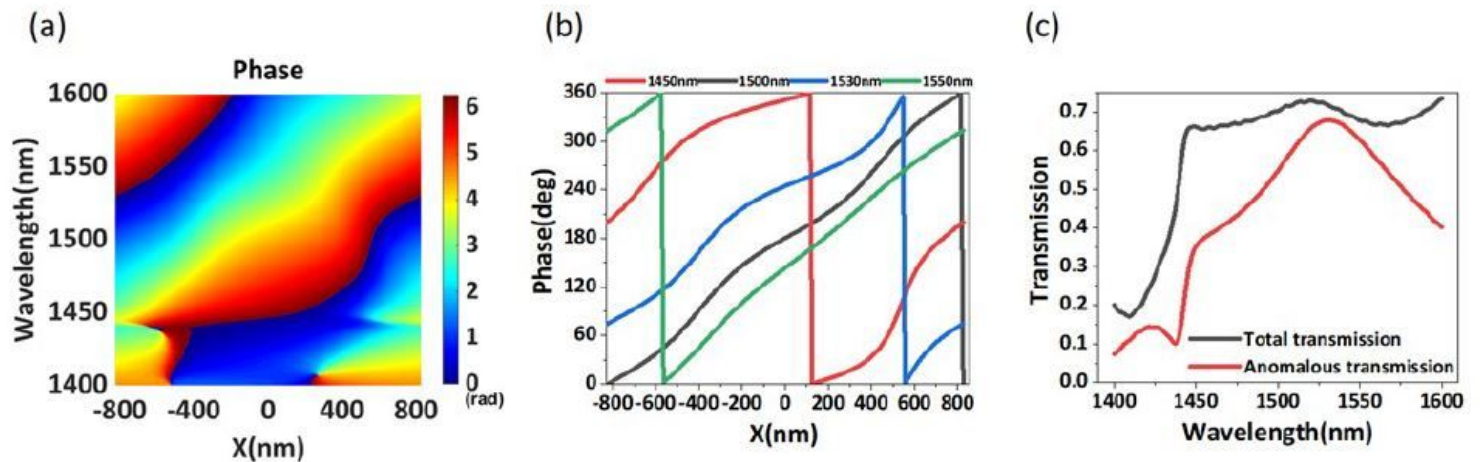


Figure 8

The convergence and optimality of the proposed algorithm.